Fractional-Order Integral Sliding-Mode Flux Observer for Sensorless Vector-Controlled Induction Motors

Yeong-Hwa Chang, Chun-I Wu, Hung-Chih Chen, Chia-Wen Chang, and Hung-Wei Lin

Abstract— The control performance of sensorless vector-controlled induction motors mainly relies on the accurate flux estimation. However, due to the variations of electrical parameters, the inaccuracy of estimated fluxes will cause the performance degradation of speed control. In this paper, a fractional-order integral sliding-mode flux observer is provided to estimate the d- and q-axis fluxes in the stationary reference frame. In addition to simulations, a DSP/FPGA based experimental platform is setup to evaluate the feasibility of the proposed scheme. Simulations and experimental results illustrate that the performance of flux and speed tracking can be performed as desire by utilizing the fractional-order integral sliding-mode flux observer in a wide speed range.

I. INTRODUCTION

The vector-controlled scheme, also called field-oriented control, made the control of AC motors equivalent to that of separately excited DC motors with certain coordinate transformations and decoupling manipulations [1]. High-performance vector-controlled induction motors without speed sensors are popularly used in industries due to the high reliability of the overall system and low cost of maintenance. The existence of flux-estimation errors will deteriorate the control performance of induction motors. Current model and voltage model are two typical flux observers which have the advantage of computation simplicity. However, the incapability of dealing with parameter variations is the common drawback [2]. The estimation accuracy and robustness of flux observers have attracted a lot of attentions in high performance induction drives. For example, a reduced-order flux observer was utilized for the speed control of induction motors by using the measurements of stator currents and rotor speeds in [3]. Hilairet *et al.* [4] proposed a two-stage extended Kalman filter for the flux and speed estimation of induction motors.

The variable structure control (VSC) strategy using the sliding-mode (SM) control theory can offer some interesting features, such as robustness to parameters variations, insensitivity to disturbances and fast dynamic responses [5]. Recently, the sliding-mode concepts have been successfully applied to high performance induction motors. For examples, Chen [6] introduced a sliding-mode flux controller and a sliding-mode speed controller to enhance the flux and speed responses of induction motors. In the work of Zaky *et al.* [7], a parallel speed and stator resistance estimation algorithm

based on a sliding-mode current observer was represented to implement a good operation of a sensorless induction motor in low speed regions. In general, the sliding-mode control system is sensitive to the parameter variations and external disturbances during the reaching phase. On the other hand, the system trajectories in the integral sliding-mode (ISM) scheme can be established without a reaching phase, and the robustness subject to parameter variations and disturbances is guaranteed starting from the initial time instance. Relative studies can be found in [8]-[9].

In most cases of sliding manifolds, the order of integration or derivation is an integer. However, subject to the increasing complexity of control systems, integer-order operators may not meet the required performance and robustness of concern. By adopting the concepts of the fractional-order calculus, it could take the advantage of the flexible selectivity of orders [10]. Podlubny [11] introduced that the fractional-order calculus could be applied to deal with the control problems of dynamic systems and to enhance the system control performance. Some applications of fractional-order sliding-mode controllers are found in references [12]-[14]. In this paper, considering the benefits of fractional-order calculus, a fractional-order integral sliding-mode (FOISM) flux observer is proposed for vector-controlled induction motors. In the proposed scheme, the differences between the observed and measured stator currents are used to define the sliding surface. Accordingly, the switching control law is designed and the system convergence is proved by the Lyapunov theorem. Furthermore, a DSP/FPGA based experimental system is set up to evaluate the feasibility of proposed works.

The organization of this paper is as follows. Section 2 briefly describes the dynamic model of induction motors. In addition, the basic concepts of fractional-order calculus and the approximation of fractional operators are discussed. In Section 3, an FOISM flux observer is addressed. Also, the speed estimation of the induction motor is investigated. Thereafter, simulation and experimental results are provided in Section 4. Finally, the concluding remarks and future works are given in Section 5.

II. PRELIMINARIES

A. Dynamic Model of Induction Motors

It is noted that the mathematical model of the vector-controlled induction motor is highly nonlinear. The dynamic model of an induction motor is commonly discussed with ignoring the parasitic effects such as magnetic saturation, eddy current, iron loss and hysteresis [15]. Based on a d-q

Y.-H. Chang, C.-I Wu, H.-C. Chen and C.-W. Chang are with the Department of Electrical Engineering, Chang Gung University, Tao-yuan, Taiwan. H.-W. Lin is with the Department of Electrical Engineering, Lee-Ming Institute of Technology, Taipei, Taiwan. (Corresponding author: Dr. Yeong-Hwa Chang, Email: `yhchang@mail.cgu.edu.tw`)

axis coordinate model in the stationary reference frame, the state equations of an induction motor can be described as [16]

$$\begin{bmatrix} \dot{i}_{ds} \\ \dot{i}_{qs} \end{bmatrix} = k_1 \left(\begin{bmatrix} \eta & \omega_r \\ -\omega_r & \eta \end{bmatrix} \begin{bmatrix} \phi_{dr} \\ \phi_{qr} \end{bmatrix} - \eta L_m \begin{bmatrix} i_{ds} \\ i_{qs} \end{bmatrix} \right)$$
$$- k_2 \begin{bmatrix} i_{ds} \\ i_{qs} \end{bmatrix} + k_3 \begin{bmatrix} v_{ds} \\ v_{qs} \end{bmatrix} \tag{1}$$

$$\begin{bmatrix} \dot{\phi}_{dr} \\ \dot{\phi}_{qr} \end{bmatrix} = - \left(\begin{bmatrix} \eta & \omega_r \\ -\omega_r & \eta \end{bmatrix} \begin{bmatrix} \phi_{dr} \\ \phi_{qr} \end{bmatrix} - \eta L_m \begin{bmatrix} i_{ds} \\ i_{qs} \end{bmatrix} \right) \tag{2}$$

where $k_1 = \frac{k_3 L_m}{L_r}$, $k_2 = \frac{R_s}{\sigma L_s}$, $k_3 = \frac{1}{\sigma L_s}$ and $\eta = \frac{R_r}{L_r}$. In (1) and (2), i, ϕ, v, R and L are the current, flux, voltage, resistance and inductance, the subscripts d and q denote the components of d- and q-axis, the subscripts r and s mean the rotor and stator, L_m is the mutual inductance between the rotor and stator, σ is the total flux leakage coefficient, and ω_r is the electrical angular speed of the rotor, respectively.

B. Fractional-Order Calculus

Fractional order calculus, developed from ordinary calculus, is a generalization of the integration and differentiation to the non-integer (fractional) order generalized operator $_aD_t^\lambda$, in which a and t are the limits and λ is the order of the operator. Two general fractional integral/differential operations are commonly discussed [17]. The first is the Grünwald-Letnikov (GL) definition

$$_aD_t^\lambda f(t) = \lim_{h \to 0} \frac{1}{h^\lambda} \sum_{j=0}^{\frac{t-a}{h}} \frac{(-1)^j \cdot \Gamma(\lambda+1)}{\Gamma(j+1) \cdot \Gamma(\lambda-j+1)} f(t-jh) \tag{3}$$

where $\Gamma(\bullet)$ is the Euler's gamma function. The other one is the Riemann-Liouville (RL) definition

$$_aD_t^\lambda f(t) = \frac{1}{\Gamma(-\lambda)} \int_a^t \frac{f(\tau)}{(t-\tau)^{\lambda+1}} d\tau \tag{4}$$

Having zero initial conditions, the Laplace transformation of the RL definition for a fractional order λ is given by

$$\mathcal{L} \left\{ _0D_t^\lambda f(t) \right\} = s^\lambda F(s) \tag{5}$$

Intuitively, the fractional-order integral/differential operator has more degrees of freedom than the ones with integer orders. It can be expected that a better performance can be obtained with the proper choice of orders. In the rest of this paper, a simplified notation D^λ is used to represent the fractional-order operator, $D^\lambda \equiv {_0D_t^\lambda}$.

C. Approximation of Fractional Operators

Practically, transfer functions with fractional-order integral/differential operators are usually approximated by integer-order transfer functions when fractional-order controllers have to be implemented, in which a close enough behavior is acquired with less complexity. Referring to [12], the approximate implementation of fractional-order controllers

can be categorized as the analog approximate implementation approach and the digital approximate implementation approach.

For example, let $[\omega_A, \omega_B]$ be the frequency range of concern. To obtain an adequate approximation of a fractional-order differential operator, the high- and low-transitional frequencies are chosen as $\omega_h \gg \omega_B$ and $\omega_b \ll \omega_A$, respectively. Then, the approximation of the frequency-band fractional differential operator can be determined as [18], [19]

$$s^\lambda \approx \left(\frac{\omega_u}{\omega_h} \right)^\lambda \prod_{k=-N}^{N} \frac{1 + s/\omega_k'}{1 + s/\omega_k} \tag{6}$$

$$\omega_k' = \omega_b \left(\frac{\omega_h}{\omega_b} \right)^{\frac{k+N+1/2-\lambda/2}{2N+1}}, \quad \omega_k = \omega_b \left(\frac{\omega_h}{\omega_b} \right)^{\frac{k+N+1/2+\lambda/2}{2N+1}}$$

in which ω_k' is the zero of rank k, ω_k is the pole of rank k, $2N+1$ is the number of zeros and poles, $\omega_u = (\omega_b \cdot \omega_h)^{1/2}$.

In practice, the approximate transformations of fractional-order operators are related to a frequency truncation. Intuitively, the degree of approximation of fractional-order operators is related to the chosen transitional frequencies and the order N. It can be expected that the approximation is more accurate with a larger N. However, the computation complexity will be increased with the increasing of N. On the other hand, with a fixed order N, the characteristics of chosen bounded frequencies are also interesting. Accordingly, to obtain a better approximation in the viewpoint of frequency responses, a wider range of $[\omega_b, \omega_h]$ is adopted.

Remark 2.1: The selections of the ranges of high- and low-transitional frequencies can cause various results of approximations. With regard to the possibility of implementation and the accuracy of approximation, above ranges should be selected adequately according to the characteristics of the controlled plants.

III. FLUX AND SPEED ESTIMATION

From (1) and (2), the conventional current mode flux observer can be represented as follows

$$\begin{bmatrix} \dot{\hat{i}}_{ds} \\ \dot{\hat{i}}_{qs} \end{bmatrix} = k_1 \begin{bmatrix} \psi_d \\ \psi_q \end{bmatrix} - k_2 \begin{bmatrix} \hat{i}_{ds} \\ \hat{i}_{qs} \end{bmatrix} + k_3 \begin{bmatrix} v_{ds} \\ v_{qs} \end{bmatrix} \tag{7}$$

$$\begin{bmatrix} \dot{\hat{\phi}}_{dr} \\ \dot{\hat{\phi}}_{qr} \end{bmatrix} = - \begin{bmatrix} \psi_d \\ \psi_q \end{bmatrix} \tag{8}$$

in which the terms ψ_d and ψ_q can be obtained as

$$\begin{bmatrix} \psi_d \\ \psi_q \end{bmatrix} = \begin{bmatrix} \eta & \omega_r \\ -\omega_r & \eta \end{bmatrix} \begin{bmatrix} \hat{\phi}_{dr} \\ \hat{\phi}_{qr} \end{bmatrix} - \eta L_m \begin{bmatrix} \hat{i}_{ds} \\ \hat{i}_{qs} \end{bmatrix} \tag{9}$$

Referring to (2), (8) and (9), it can be seen that the flux estimation could be affected by the parameter variations of R_r and L_r. In this paper, an FOISM observer is proposed to improve the performance of flux estimation. Based on the current errors, $\tilde{i}_d = \hat{i}_{ds} - i_{ds}$, $\tilde{i}_q = \hat{i}_{qs} - i_{qs}$, between the

measured and estimated stator currents, the sliding surface of the FOISM flux observer is defined in the following

$$\mathbf{S} = \left[\begin{array}{c} s_d \\ s_q \end{array} \right] = \left[\begin{array}{c} c_1 \tilde{i}_d + c_2 D^{-\lambda} \tilde{i}_d \\ c_1 \tilde{i}_q + c_2 D^{-\lambda} \tilde{i}_q \end{array} \right] \tag{10}$$

where c_1 and c_2 are positive constants. In (10), $D^{-\lambda}$ is considered as a fractional-order integral operator with $\lambda \in (0, 1]$. From (9) and (10), the derivative of $\mathbf{S}$ can be derived as follows

$$\begin{aligned} \dot{\mathbf{S}} &= c_1 \left[\begin{array}{c} \dot{\hat{i}}_{ds} - \dot{i}_{ds} \\ \dot{\hat{i}}_{qs} - \dot{i}_{qs} \end{array} \right] + c_2 D^{-\lambda+1} \left[\begin{array}{c} \tilde{i}_d \\ \tilde{i}_q \end{array} \right] \\ &= c_1 k_1 \left[\begin{array}{c} \psi_d \\ \psi_q \end{array} \right] + c_1 k_1 \left[\begin{array}{c} M \\ N \end{array} \right] - c_1 k_2 \left[\begin{array}{c} \tilde{i}_d \\ \tilde{i}_q \end{array} \right] \\ &\quad + c_2 D^{-\lambda+1} \left[\begin{array}{c} \tilde{i}_d \\ \tilde{i}_q \end{array} \right] \end{aligned} \tag{11}$$

where $M = -\eta \phi_{dr} - \omega_r \phi_{qr} + \eta L_m i_d$ and $N = \omega_r \phi_{dr} - \eta \phi_{qr} + \eta L_m i_q$. In the proposed FOISM flux observer, ψ_d and ψ_q can be designed by the Lyapunov method. Considering $V = \frac{1}{2} \mathbf{S}^T \mathbf{S}$ as the Lyapunov function candidate, the derivative of V can be described in the following

$$\begin{aligned} \dot{V} &= \mathbf{S}^T \dot{\mathbf{S}} \\ &= \mathbf{S}^T \left\{ c_1 k_1 \left[\begin{array}{c} \psi_d \\ \psi_q \end{array} \right] + c_1 k_1 \left[\begin{array}{c} M \\ N \end{array} \right] - c_1 k_2 \left[\begin{array}{c} \tilde{i}_d \\ \tilde{i}_q \end{array} \right] \right. \\ &\quad \left. + c_2 D^{-\lambda+1} \left[\begin{array}{c} \tilde{i}_d \\ \tilde{i}_q \end{array} \right] \right\} \end{aligned} \tag{12}$$

Assume that $\max |c_1 k_1 M| < Q_d < \infty$ and $\max |c_1 k_1 N| < Q_q < \infty$. It can be obtained that $s_d \cdot \max |c_1 k_1 M| < s_d \cdot sign(s_d) Q_d$ and $s_q \cdot \max |c_1 k_1 N| < s_q \cdot sign(s_q) Q_q$. Then (12) can be rewritten as

$$\begin{aligned} \dot{V} &< \mathbf{S}^T \left\{ c_1 k_1 \left[\begin{array}{c} \psi_d \\ \psi_q \end{array} \right] - c_1 k_2 \left[\begin{array}{c} \tilde{i}_d \\ \tilde{i}_q \end{array} \right] + \left[\begin{array}{c} sign(s_d) Q_d \\ sign(s_q) Q_q \end{array} \right] \right. \\ &\quad \left. + c_2 D^{-\lambda+1} \left[\begin{array}{c} \tilde{i}_d \\ \tilde{i}_q \end{array} \right] \right\} \end{aligned} \tag{13}$$

From (13), the stabilizing control law can be defined as

$$\begin{aligned} \left[\begin{array}{c} \psi_d \\ \psi_q \end{array} \right] &= \frac{k_2}{k_1} \left[\begin{array}{c} \tilde{i}_d \\ \tilde{i}_q \end{array} \right] - \frac{u_0}{c_1 k_1} \left[\begin{array}{c} sign(s_d) \\ sign(s_q) \end{array} \right] \\ &\quad - \frac{c_2}{c_1 k_1} D^{-\lambda+1} \left[\begin{array}{c} \tilde{i}_d \\ \tilde{i}_q \end{array} \right] \end{aligned} \tag{14}$$

where $sign(s_j) = s_j / |s_j|$, $j \in \{d, q\}$, if $s_j \neq 0$, $sign(s_j) = 0$, otherwise, and u_0 is a positive constant gain.

Theorem 3.1: The sliding mode of the induction motor using the proposed FOISM flux observer is guaranteed if the constant gain u_0 of the control law (14) is satisfied with $u_0 > \max [Q_d, Q_q]$.

Proof: Substituting ψ_d and ψ_q of (14) into (13), it gives that

$$\dot{V} \leq \left[\begin{array}{c} s_d \\ s_q \end{array} \right]^T \left(- \left[\begin{array}{c} u_0 \cdot sign(s_d) \\ u_0 \cdot sign(s_q) \end{array} \right] + \left[\begin{array}{c} sign(s_d) Q_d \\ sign(s_q) Q_q \end{array} \right] \right)$$

$$= - [s_d \cdot sign(s_d)(u_0 - Q_d) + s_q \cdot sign(s_q)(u_0 - Q_q)]$$

It could be obtained that $u_0 - Q_d > 0$ and $u_0 - Q_q > 0$ because of the assumption $u_0 > \max [Q_d, Q_q]$. Therefore, we can conclude that $\dot{V} < 0$, i.e. the sliding mode of the FOISM flux estimation is guaranteed. ∎

It is noted that the convergence of the flux observer can be ensured by selecting a large enough u_0 according to the constraint $u_0 > \max [Q_d, Q_q]$. However, an excessively large u_0 may produce a high control signal that could yield saturations of the driver. When the system trajectories reach to the sliding surface, i.e. $\mathbf{S} = [0, 0]^T$, the d- and q-axis observed currents will converge to the actual currents. Accordingly, the errors of flux estimation will also tend to zeros.

It is well known that the sliding-mode method suffers from the problem of chattering, which can excite unexpected high frequency responses. In this paper, a saturation function is adopted to eliminate the chattering effects as follows [20]

$$sat(s_j) = \left\{ \begin{array}{ll} sign(s_j/\varepsilon), & \text{if } |s_j/\varepsilon| \geq 1 \\ s_j/\varepsilon, & \text{if } |s_j/\varepsilon| < 1 \end{array} \right. , \ j \in \{d, q\} . \tag{15}$$

where $\varepsilon > 0$ represents the thickness of the boundary layer. From (14) and (15), the FOISM flux observer with the saturation function can be described as follows

$$\left[\begin{array}{c} \psi_d \\ \psi_q \end{array} \right] = \left[\begin{array}{c} -\frac{1}{c_1 k_1} u_0 \cdot sat(s_d) + \frac{k_2}{k_1} \tilde{i}_d - \frac{c_2}{c_1 k_1} D^{-\lambda+1} \tilde{i}_d \\ -\frac{1}{c_1 k_1} u_0 \cdot sat(s_q) + \frac{k_2}{k_1} \tilde{i}_q - \frac{c_2}{c_1 k_1} D^{-\lambda+1} \tilde{i}_q \end{array} \right] \tag{16}$$

Remark 3.1: The integral sliding mode flux observer is a special case of the proposed FOISM flux observer, where λ is set to 1.

Remark 3.2: It is observed that the larger ε is, the less chattering phenomenon is. However, the steady-state error will be arisen as ε increasing. Therefore, the choice of ε is a trade-off between the chattering phenomenon and the steady-state error.

Remark 3.3: Given $0 < \lambda \leq 1$, it can be obtained that $-\lambda+1 \in [0, 1)$. Thus, from (16), the proposed control actions consist of fractional-order differential terms. In fact, both the operations of fractional-order integral and differential operators are embedded in the control actions, where the integral terms are inherited in the sliding surfaces, s_d and s_q.

The estimated rotor speed of the induction motor is derived from the results of the flux estimation. From (9), the speed estimation can be obtained in the following

$$\left[\begin{array}{c} \psi_d \\ \psi_q \end{array} \right] = \left[\begin{array}{cc} \eta & \hat{\omega}_r \\ -\hat{\omega}_r & \eta \end{array} \right] \left[\begin{array}{c} \hat{\phi}_{dr} \\ \hat{\phi}_{qr} \end{array} \right] - \eta L_m \left[\begin{array}{c} \hat{i}_{ds} \\ \hat{i}_{qs} \end{array} \right] \tag{17}$$

From (17), the estimated speed of the induction motor can be described in the following

$$\hat{\omega}_r = \frac{\hat{\phi}_{qr} \psi_d - \hat{\phi}_{dr} \psi_q - \eta L_m \left(\hat{i}_{qs} \hat{\phi}_{dr} - \hat{i}_{ds} \hat{\phi}_{qr} \right)}{\hat{\phi}_{dr}^2 + \hat{\phi}_{qr}^2} \tag{18}$$

Fig. 1. The block diagram of the proposed scheme.

$$\hat{\omega}_{rm} = \frac{2}{N_p}\hat{\omega}_r \qquad (19)$$

where N_p is the number of poles and $\hat{\omega}_{rm}$ is the estimated mechanical angular speed of the rotor. Consequently, the block diagram for the sensorless vector-controlled induction motor with the proposed FOISM flux observer is depicted in Fig. 1.

IV. SIMULATION AND EXPERIMENTAL RESULTS

In this paper, a three-phase 0.1 kW squirrel cage induction motor is used, and the physical parameters are shown in Table I. The motor is driven by a sinusoidal pulse-width modulation (SPWM) inverter of which the switching frequency and dead time are 10 kHz and 3 μs, respectively. Regarding to the switching frequency, the required transitional frequencies for the approximation of integral/differential operators are set to $\omega_h = 10^4\ rad/sec$ and $\omega_b = 10^{-4}\ rad/sec$. Simulations are performed by Matlab to validate the performance of the proposed FOISM observer. The speed, flux and current controllers of the vector-controlled scheme are designed based on the Ziegler-Nichols algorithm. Following the proposed design procedures, the relative coefficients of relative controllers and observers are summarized in Table II. In current study, the control responses of flux and speed tracking are mainly addressed where the flux observers are utilized in the presence of different speed commands and load conditions. Three types of flux observers, SM, ISM and FOISM, are considered, in which the speed, flux and current controllers remain identically. In addition, the simulation results are presented by calculating the root-mean-square (RMS) values of tracking errors. To highlight the feasibility and superiority of the proposed scheme, forward-reverse operations are implemented to validate the capability of dealing with load disturbances, where extrogenous loads are applied on t = 3, 13, 23, 33 second and removed on t = 7, 17, 27, 37 second. In the meantime, the flux and load torque commands are set to 0.22 wb and 0.15 Nt-m, respectively. The simulation results of steady-state tracking errors of flux and speed estimations are summarized in Table III. It is observed that the flux and speed tracking errors of the FOISM flux observer are smaller than the counterparts of other flux observers.

As shown in Fig. 2, a DSP and FPGA based experimental system with a sampling period of 1ms is set up to validate the proposed results. In the experimental platform, the TMS320C6713 DSP board is used to implement all control algorithms coded with C language, and the Stratix EP1S25 FPGA board is used to implement all functions of data bus, encoder, A/D converter and SPWM inverter. The induction motor used in the experiment is a Nikki Denso NF21-3F three-phase squirrel cage machine. The external load torque is produced by a Mitsubishi ZKG-10AN powder clutch. The hardware implementations are provided with the same manners of simulations. The flux responses corresponding to SM, ISM and FOISM flux observers on $\omega_{rm}^* = 1800$ rpm and 500 rpm are shown in Fig. 3 and Fig. 4, respectively. From these experimental results, it can be seen that responses of the proposed FOISM flux observer are better than other flux observers via different speed commands. Furthermore, the speed responses with different flux observers on $\omega_{rm}^* = 1800$ rpm and 500 rpm are shown in Fig. 5 and Fig. 6. It is noted that the FOISM flux observer can provide good speed responses in the aspect of tracking accuracy. With regard to different speed commands, 500, 900 and 1800 rpm, the speed transient responses with load suddenly applied are

TABLE III

THE SIMULATION RESULTS OF STEADY-STATE TRACKING ERRORS OF
FLUX AND SPEED ESTIMATIONS.

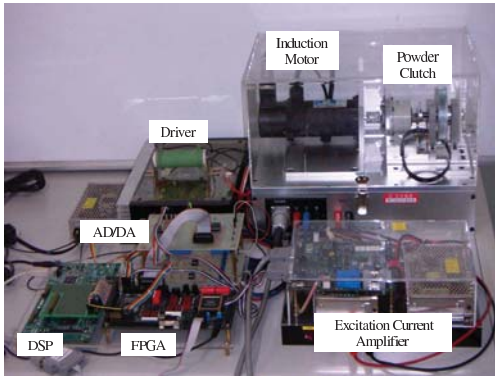| ω_{rm}^* (rpm)	Methods	Flux error (wb)	Speed error (rpm)
1800	SM [16]	0.0068	7.5183
	ISM	0.0066	7.3186
	FOISM	0.0064	7.1572
900	SM	0.0060	5.8224
	ISM	0.0055	5.7071
	FOISM	0.0052	5.4616
500	SM	0.0059	5.5491
	ISM	0.0053	5.3358
	FOISM	0.0051	5.1925

Fig. 2. Experimental system setup.

TABLE IV
THE EXPERIMENTAL RESULTS OF SPEED TRANSIENT RESPONSES WITH
LOAD SUDDENLY APPLIED.

ω_{rm}^* (rpm)	Methods	Instant error (rpm)	Recovery time (sec)
	SM	65.1678	0.91
1800	ISM	47.7489	0.72
	FOISM	42.6475	0.49
	SM	51.6187	0.72
900	ISM	43.8975	0.61
	FOISM	35.7514	0.46
	SM	42.5768	0.55
500	ISM	31.9428	0.46
	FOISM	24.8067	0.38

Fig. 3. The experimental flux responses corresponding to different flux observers, $\omega_{rm}^* = 1800$ rpm: (a) SM, (b) ISM, (c) FOISM.
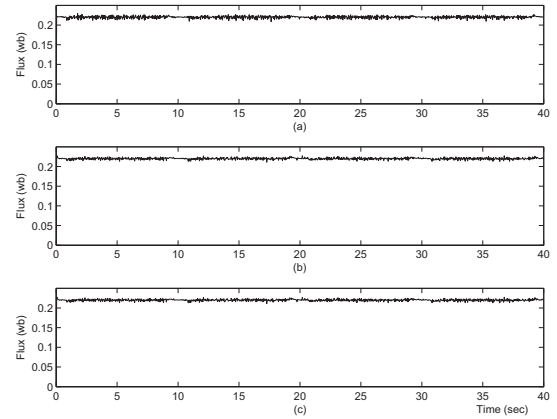

Fig. 4. The experimental flux responses corresponding to different flux observers, $\omega_{rm}^* = 500$ rpm: (a) SM, (b) ISM, (c) FOISM.

listed in Table IV. It can be observed that the instant speed error and recovery time with the FOISM flux observer are the smallest among three estimation schemes subject to load disturbances. Moreover, the steady-state responses of speed and flux tracking are tabulated in Table V. It is apparent that the speed and flux tracking errors with the FOISM flux observer are less than the counterparts of other observers. From Table IV and Table V, it can be summarized that the proposed FOISM flux observer can provide much better control responses in both transient and steady-state manners with various speed commands and extrogenous loads.

TABLE V
THE EXPERIMENTAL RESULTS OF STEADY-STATE RESPONSES WITH
LOAD APPLIED.

ω_{rm}^* (rpm)	Methods	Flux error (wb)	Speed error (rpm)
	SM	0.0088	28.0325
1800	ISM	0.0073	25.3599
	FOISM	0.0061	16.4656
	SM	0.0085	13.2224
900	ISM	0.0068	10.1751
	FOISM	0.0057	6.4744
	SM	0.0081	11.8234
500	ISM	0.0067	8.8286
	FOISM	0.0058	5.9311

V. CONCLUSIONS

In this paper, an induction motor based on the sensorless vector-controlled scheme is discussed, where the flux/speed estimation and tracking are the main subjects of concern. A fractional-order integral sliding-mode flux observer is proposed to take the advantage of the flexibility of the fractional orders, and the associated performance of speed control is investigated. A DSP/FPGA based experimental system is setup to validate the feasibility of the proposed works. Compared to the integer-order flux observers, simulation and experimental results illustrate that the proposed FOISM flux observer can achieve much better performance in both the steady-state and transient responses subject to load disturbances. Also, the tracking performance of vector-controlled induction motors is getting better if a relatively robust and accurate flux observer is provided. This paper has discussed the flux estimation with certain fractional orders of the integral/differential operators. Therefore, how to get the optimal values of the fractional orders will be involved in the future research works, where an optimization framework might be a promising challenge.
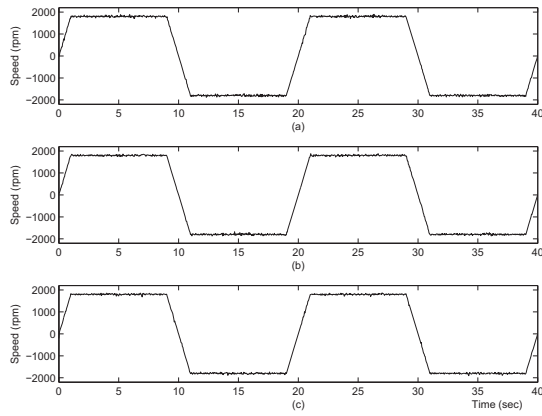
Fig. 5. The experimental speed responses corresponding to different flux observers, $\omega_{rm}^* = 1800$ rpm: (a) SM, (b) ISM, (c) FOISM.
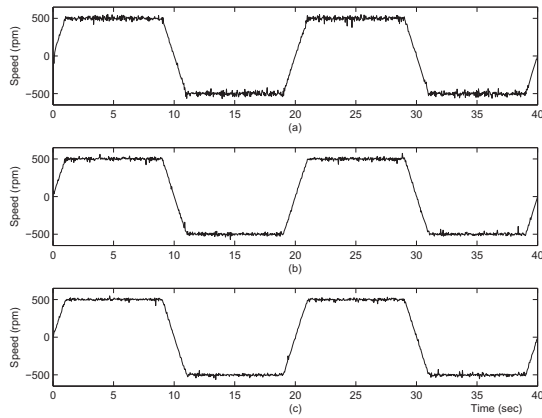

Fig. 6. The experimental speed responses corresponding to different flux observers, $\omega_{rm}^* = 500$ rpm: (a) SM, (b) ISM, (c) FOISM.

REFERENCES

[1] Y.-H. Chang, Y.-Y. Wang, M.-H. Hung, and P.-C. Chen, "Regional stability and H_∞ performance control of an input-saturated induction motor via LMI approach," *Asian Journal of Control*, vol. 7, no. 4, pp. 368-379, 2005.

[2] N. Inanc, "A new sliding mode flux and current observer for direct field oriented induction motor drives," *Electric Power Systems Research*, vol. 63, no. 2, pp. 113-118, 2002.

[3] F. Alonge and F. D'Ippolito, "Design and sensitivity analysis of a reduced-order rotor flux optimal observer for induction motor control," *Control Engineering Practice*, vol. 15, no. 12, pp. 1508-1519, 2007.

[4] M. Hilairet, F. Auger, and E. Berthelot, "Speed and rotor flux estimation of induction machines using a two-stage extended Kalman filter," *Automatica*, vol. 45, no. 8, pp. 1819-1827, 2009.

[5] K. D. Young, V. I. Utkin, and Ü. Özgüner, "A control engineers guide to sliding mode control," *IEEE Trans. on Control Systems Technology*, vol. 7, no. 3, pp. 328-342, May 1999.

[6] C.-Y. Chen, "Sliding mode controller design of induction motor based on space-vector pulsewidth modulation method," *International Journal of Innovative Computing, Information and Control*, vol. 5, no. 10(B), pp. 3603-3614, Oct. 2009.

[7] M. S. Zaky, M. Khater, H. Yasin, and S. S. Shokralla, "Very low speed and zero speed estimations of sensorless induction motor drives," *Electric Power Systems Research*, vol. 80, no. 2, pp. 143-151, 2010.

[8] V. I. Utkin and J. Shi, "Integral sliding mode in systems operating under uncertainty conditions," *Proceedings of the 35th Conference on Decision and Control*, pp. 4591-4596, Kobe, Japan, Dec. 1996.

[9] M. Jiménez-Lizárraga and L. Fridman, "Robust Nash strategies based on integral sliding mode control for a two players uncertain linear affine-quadratic game," *International Journal of Innovative Computing, Information and Control*, vol. 5, no. 2, pp. 241-251, Feb. 2009.

[10] C. Ma and Y. Hori, "Fractional-order control: Theory and applications in motion control," *IEEE Trans. on Industrial Electronics Magazine*, vol. 1, no. 4, pp. 6-16, 2007.

[11] I. Podlubny, "Fractional-order systems and $PI^\lambda D^\mu$-controllers," *IEEE Trans. on Automatic Control*, vol. 44, no. 1, pp. 208-214, Jan. 1999.

[12] A. J. Calderón, B. M. Vinagre, and V. Feliu, "Fractional order control strategies for power electronic buck converters," *Signal Processing*, vol. 86, no. 10, pp. 2803-2819, Oct. 2006.

[13] M. Ö. Efe, "Fractional fuzzy adaptive sliding-mode control of a 2-DOF direct-drive robot arm," *IEEE Trans. on Systems, Man, and Cybernetics-Part B: Cybernetics*, vol. 38, no. 6, pp. 1561-1570, Dec. 2008.

[14] H. Delavari, R. Ghaderi, A. Ranjbar, and S. Momani, "Fuzzy fractional order sliding mode controller for nonlinear systems," *Communications in Nonlinear Science and Numerical Simulation*, vol. 15, no. 4, pp. 963-978, Apr. 2010.

[15] E. Laroche, E. Sedda, and C. Durieu, "Methodological insights for online estimation of induction motor parameters," *IEEE Trans. on Control System Technology*, vol. 16, no. 5, pp. 1021-1028, Sept. 2008.

[16] H. Rehman, A. Derdiyok, M. K. Guven, and L. Xu, "A new current model flux observer for wide speed range sensorless control of an induction machine," *IEEE Trans. on Power Electronics*, vol. 17, no. 6, pp. 1041-1048, Nov. 2002.

[17] I. Podlubny, *Fractional Differential Equations*, Academic Press, San Diego, CA, 1999.

[18] A. Oustaloup, F. Levron, B. Mathieu, and F. M. Nanot, "Frequency-band complex noninteger differentiator: Characterization and synthesis," *IEEE Trans. on Circuits and Systems-I: Fundamental Theory and Applications*, vol. 47, no. 1, pp. 25-39, 2000.

[19] B. Vinagre, I. Podlubny, A. Hernandez, and V. Feliu, "Some approximations of fractional order operators used in control theory and applications," *Fractional Calculus & Applied Analysis*, vol. 3, no. 3, pp. 231-248, 2000.

[20] M. Demirtas, "DSP-based sliding mode speed control of induction motor using neuro-genetic structure," *Expert Systems with Applications*, vol. 36, no. 3(I), pp. 5533-5540, 2009.